Report
P-17-25
May 2018

Seismic reflection, refraction and tomography results from 3D seismic data, Forsmark

Emil Lundberg
Christopher Juhlin
Fengjiao Zhang
Ruth Behrendt

SVENSK KÄRNBRÄNSLEHANTERING AB

SWEDISH NUCLEAR FUEL
AND WASTE MANAGEMENT CO

Box 3091, SE-169 03 Solna
Phone +46 8 459 84 00
skb.se

SVENSK KÄRNBRÄNSLEHANTERING

ISSN 1651-4416
SKB P-17-25
ID 1592845
May 2018

Seismic reflection, refraction and tomography results from 3D seismic data, Forsmark

Emil Lundberg, Christopher Juhlin, Fengjiao Zhang, Ruth Behrendt

Uppsala University, Department of Earth Sciences

Summary

As a part of the investigations for the planned Spent Fuel Repository, a 3D seismic dataset was acquired in Forsmark, Sweden in August 2016. Seismic data was processed both with refraction processing and tomography, which aims at characterizing the near surface conditions including depth to bedrock and low velocity zones in the bedrock. Tomography and refraction processing can detect low velocity zones, which reaches the surface or the top of the bedrock with a steep inclination. Low velocity bedrock may indicate fractured rock, which may have implications for the construction of entrance tunnels and infrastructure for the Spent Fuel Repository. Reflection seismic processing was also performed, with the aim of imaging possible structures at deeper level between the top of the bedrock down to about 500 m depth. Structures that may give rise to reflections are for example lithological changes and deformation zones. Shallow dipping structures or subhorizontal structers are more easily detected with reflection processing.

The bedrock depth varied between 3 m above sea level to 7 m below sea level. Depth were compared with results from geotechnical drilling and showed good agreement in most cases. Deepest sediment/bedrock interface were found in the northern part of the 3D area and in a narrow zone towards south. Low velocity bedrock showed a similar trend with low velocities mainly in the north and towards the south. Low velocity bedrock may indicate fractured bedrock.

Most reflectivity occurred between 40 and 80 m depth, but also continuing down to about 200 m depth in some parts. Based on previous seismic investigations it was hypothesized that the deformation zone ZFM1203 potentially could continue as a shallow dipping structure beneath the 3D area. It was also suggested that reflections in the area could relate to a boundary between fractured bedrock and intact bedrock. There is a clear relationship with the uppermost reflectivity, at about 40 to 60 m depth in the stacked 3D seismic data, and interpreted intersections between fracture domains FFM01 and FFM02. The deeper reflections can, however not be explained by the boundary between these fracture domains. Modelling a structure dipping 8° towards northwest and originating at the surface location of ZFM1203 produced a structure that appears to match some of the deeper reflectivity in the 3D seismic data. Difficulties in tracing the reflections in the 3D seismic data may arise from gaps in the data causing low fold and areas with low velocity rocks (fractured rocks), potentially masking the reflected energy. In order to verify if ZFM1203 is continuing beneath the 3D area a profile that reaches the surface expression of the deformation zone is preferred, this may however be challenging in practice since the area between the 3D area and ZFM1203 is a mixture of land and marine environment. More of the reflectivity seen between 40 and 200 m depth may be explained by incorporating a better downhole velocity profiles.

Further mapping of sonic velocities in existing boreholes can help determining the boundary between fracture domains at the location of the boreholes. By logging the seismic velocity also at seismic wavelength by downhole hydrophones, a better depth conversion for the stacked 3D seismic data and, hence, a better image in between existing boreholes can be obtained. This type of velocity information can also give a better starting model for detailed tomography inversions along selected 2D lines with dense shot and receiver spacing.

Sammanfattning

Som en del av undersökningarna för planerandet av ett slutförvar för använt kärnbränsle utfördes ett 3D-seismiskt mätprogram i Forsmark, Sverige i augusti 2016. Insamlade seismiska data bearbetades med avseende på refraktion och tomografi, vilka syftar till att karakterisera ytnära bergförhållanden inklusive djup till bergytan och låghastighetszoner i ytberget. Meg hjälp av tomografi och refraktions processering kan man upptäcka låghastighetszoner som når till ytan eller nära bergytan med en brant lutning. Låg seismisk hastighet i berggrunden kan indikera sprickighet i berget, som kan medföra konsekvenser för byggandet av nedfartstunnlar och annan infrastruktur för Kärnbränsleförvaret. Reflektionsseismisk processering av data utfördes också, i syfte att avbilda möjliga strukturer på djupare nivå ner till ca 500 m djup. Strukturer som kan ge upphov till reflektioner är till exempel litologiska förändringar och deformationszoner. Svagt lutande eller sub-horisontella strukturer är lättare att detektera med reflektionsseismik än branta strukturer.

Bergytans nivå varierade mellan 3 m över havet och 7 m under havsnivån. Djupet från markytan till bergytan jämfördes med resultat från geotekniska borrningar i området och det visade sig i de flesta fall överensstämma väl. Det djupaste sediment /berggränssnittet hittades i den norra delen av 3D-området och i en smal zon mot söder. Områden där seismiska hastigheterna i ytberget var låga uppvisade en liknande trend, huvudsakligen i norr och mot söder. Låghastighetsområden i ytberget kan indikera sprickig berggrund.

Mest reflektivitet uppstod mellan 40 till 80 meters djup, som i vissa områden fortsätter ner till ca 200 meters djup. Baserat på tidigare seismiska undersökningar antogs det att deformationszonen ZFM1203 potentiellt kan fortsätta som en svagt lutande struktur under 3D-området. Reflektioner i området föreslogs också kunna relatera till en gräns mellan sprickig och intakt berggrund. Det finns ett tydligt samband med den översta reflektiviteten, vid ca 40 till 60 meters djup i summerade 3D-seismiska resultaten och tolkade gränsen mellan frakturdomänerna FFM01 och FFM02. De djupare reflektionerna kan emellertid inte förklaras av gränsen mellan dessa sprickdomäner. Genom att modellera en struktur som lutar 8° mot nordväst och med start vid struktur ZFM1203:s skärning med markytan producerades en struktur som tycks matcha med en del av den djupare reflektiviteten i 3D-seismiken. Svårigheter att spåra reflektionerna i 3D-seismiska data kan uppstå genom luckor i data vilka orsakar låg täckning i dessa områden samt lägen med låghastighetsberg (sprickor) som potentiellt maskerar den reflekterade energin. För att kunna verifiera om ZFM1203 fortsätter under 3D-området, föreslås en mätprofil som når från zonens ytposition till 3D-området, detta kan emellertid vara utmanande i praktiken eftersom området mellan 3D-området och ZFM1203 är en blandning av mark- och havsmiljö. Mer av reflektiviteten som ses mellan 40 och 200 meters djup kan förklaras genom bättre hastighetsprofiler ifrån borrhål.

Ytterligare kartläggning av akustiska hastigheter i befintliga borrhål kan bidra till att bestämma gränsen mellan sprickdomäner vid borrhålen. Genom att logga den seismiska hastigheten också vid seismisk våglängd genom borrhålshydrofoner, kan en bättre djupkonvertering göras för summerade 3D-seismiska data, och en bättre bild mellan befintliga borrhål erhållas. Denna typ av hastighets-information kan också ge en bättre startmodell för detaljerade tomografiska inversioner längs utvalda 2D-linjer med täta sändar- och mottagaravstånd.

Contents

1 Introduction

Forsmark, eastern Sweden, has been selected for hosting Swedish spent nuclear fuel. As a part of the investigations for the planned Spent Fuel Repository, a 3D seismic dataset was acquired, in August 2016. The main repository will be located at about 500 m depth. The bedrock in the area has been thoroughly investigated by means of geological and geophysical measurements including several seismic profiles. The 3D seismic profiles aim at more thoroughly investigating the near surface conditions at the site of the planned repository. Main targets are depth to bedrock and deformation zones affecting the construction of entrance tunnels down to the depth of the repository i.e. the upper 500 m.

Seismic data measures the velocity of seismic waves in the subsurface and can also measure the occurrence of seismic impedance contrasts in the subsurface. An impedance contrast is where the seismic velocity and/or density changes rapidly such as in a contact between different rocks or in deformation zones. The contact between sediment and bedrock gives a strong impedance contrast, too. An impedance contrast is causing seismic waves to reflect back to the surface and the reflection seismic processing aims at imaging subsurface structures based on the reflected seismic waves. The refraction and the tomography processing aims at distinguish differences in the seismic velocity in the subsurface. The strongest change in seismic velocity occurs at the boundary between bedrock and sediment. P-wave velocity in sediments can vary between very low, around 300 m/s in for example dry sand/gravel and up to approximately 2 500 m/s in for example saturated till. Bedrock velocities are in the range of 5 000–6 000 m/s. Very dense rocks may have even higher seismic velocities. In fractured rocks the seismic velocity is lower mainly due to the increased porosity and hence lower density. Fractured bedrock may have a velocity of up to 4 500 m/s. Refraction processing is good for finding strong contrasts in velocity such as the boundary between sediments and bedrock. Tomography processing is used to find low velocity zones in the bedrock indicative of fractured bedrock. The reflection processing is best for finding deeper targets such as deformation zones in bedrock and lithological changes. Therefore, the different types of processing complement each other.

This report will briefly describe the data acquisition and processing in chapters 2 and 3 respectively. The main results are presented in chapter 4 and constitute:

- Depth to bedrock, based mainly on the refraction processing.
- Near surface fracture zones. Characterized based on low velocity zones from tomography and refraction processing results.
- Deep structures (about 40 meter below sea-level and deeper), based on reflection seismic processing.

The results are compared with previously acquired reflection/refraction seismic data from 2011. About 400 geotechnical boreholes provided by SKB (B. Hansson et al. 2008; S. Hellgren 2012a; S. Hellgren 2012b) have also been used for comparison. For interpretation of reflections, 15 deep boreholes have been used (Carlsten et al. 2005, 2006, 2007). In chapter 5 interpretations of the results are provided and also uncertainties and ambiguities between borehole data and seismic data are discussed.

Refraction and reflection processing was performed using GLOBE Claritas TM under license from the Institute of Geological and Nuclear Sciences Limited, Lower Hutt, New Zealand. Travel time tomography was performed using 3D PStomo_eq code developed by Ari Tryggvason, Uppsala University and GMT from P. Wessel and W. H. F. Smith was used for preparing some of the figures.

2 Data acquisition

The seismic data was acquired with 10 Hz geophones distributed in 24 receiver lines. The receiver spacing was 4 m and inline spacing was 14 m, and six extra shot lines were added giving a total area of about 320 × 406 m covered by the 3D seismic acquisition (Figure 2-1). Receiver points are numbered from west to east and from north to south. Western most receiver line is 4 with point 401 towards north and 480 towards south. Last receiver line is 27. For reflection processing the 3D area is divided into Common Depth Point (CDP; Figure 2-2). In each CDP position traces imaging the same subsurface location are stacked to enhance the reflected signal. CDP inline direction is parallel to receiver lines. Data was acquired in four patches. Each patch was recorded with six receiver lines and a maximum of 480 receivers. Total area covered by each patch was 320 × 112 m and maximum offset between shot and receiver of approximately 340 m. To obtain overlap between the patches, three shot-lines were repeated on each side of the acquired patch. Most shot points acquired using Bobcat source were also repeated for all patches. Some Bobcat shots were performed at larger distance from the active patch resulting in some shots with a larger offset between shot and receiver. Source points along roads and in open areas around houses and in parking area were shot using Bobcat. Each point was hit about ten times and recorded during 30 s. The individual hits were then picked and stacked using a shift and stack procedure, giving a stronger source signal with reduced noise. For shot points in forest, or where access with Bobcat was impossible, dynamite was used. Charge sizes were most often 60 g, but ranging between 40 and 80 g. Shot holes were prepared using iron bar and depth varied between 0.3 m and 0.5 m. Bobcat shot points are marked in red and explosive shot points are marked in yellow in Figure 2-1. Acquisition parameters are displayed in Table 2-1. Figure 2-3 shows example shot-gathers from shot points using Bobcat single hit and stacked 7 hits as well as a shot using dynamite source. Shot points are located on line 21 and 4 m apart. The single hit Bobcat shot has higher amplitudes and first arrivals are clearer in far offsets as compared to the explosive shot (cf. Figures 2-3a and 2-3c). The stacking of several hits helps to remove uncorrelated noise and the quality of first arrivals improves; cf. Figures 2-3a and 2-3b. Figure 2-4 shows the frequency content for the stacked Bobcat shot and the explosive shot. For frequencies in the range of 50 to 80 Hz the amplitudes are significantly higher in the Bobcat shot, however at the higher frequencies in the 120 to 240 Hz range the amplitudes are higher in the explosive shots. For reflection seismic processing, higher frequency content enables a more accurate subsurface imaging, but for tomography and refraction processing, however, picking of more first arrivals is crucial for the modelling.

An important part of the setup is the surveying of shot points and receiver points. In open areas, points were surveyed using a Differential GPS (DGPS), which utilize corrections from a base station provided in real time, for a more accurate positioning. Points in the forest were surveyed using a total station and a few points were interpolated. All points were compared with 2 × 2 m gridded Lidar data to avoid any large elevation mistakes in the final data. Wrong elevations of points, especially if occurring in larger segments, are more likely to cause unwanted anomalies in seismic data than misplaced points in horizontal position; therefore, a check against accurate Lidar data ensures no human errors affect the final data.

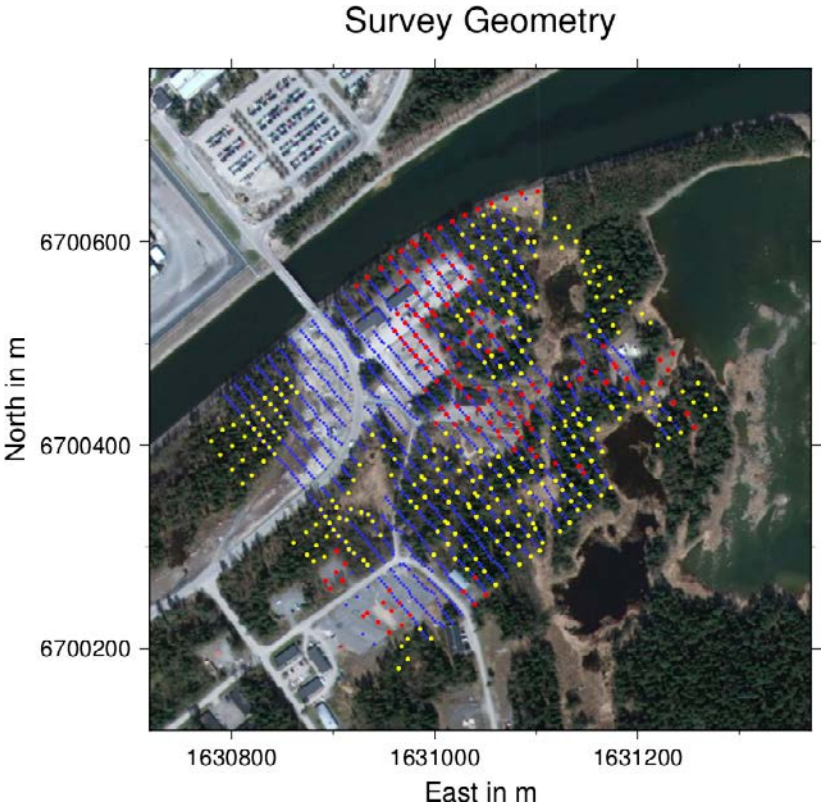

Figure 2-1. *Location of shot and receiver points. Receiver positions are marked in blue. Bobcat shot points are marked in red and Explosive shot points are marked in yellow. Receiver points are numbered from west to east and from north to south. Western most receiver line is 4 with point 401 towards north and 480 towards south. Last receiver line is 27. Coordinate system: RT90 2.5 gon W.*

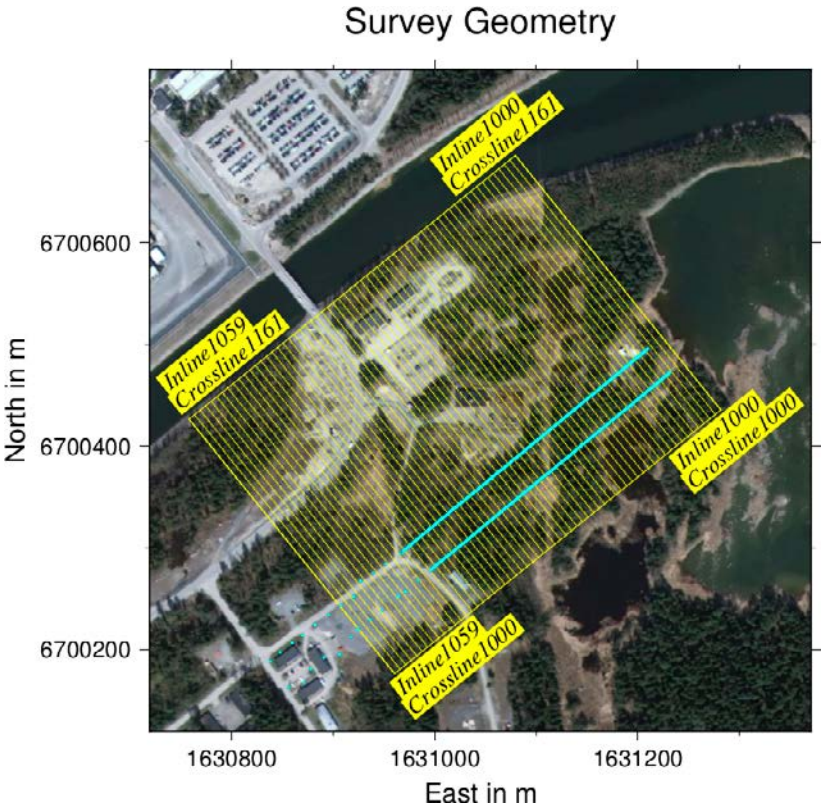

Figure 2-2. *Location of CDP positions in yellow. Blue dots/lines mark location for 2D seismic refraction/ reflection survey 2011 (Brojerdi et al. 2014). Coordinate system: RT90 2.5 gon W.*

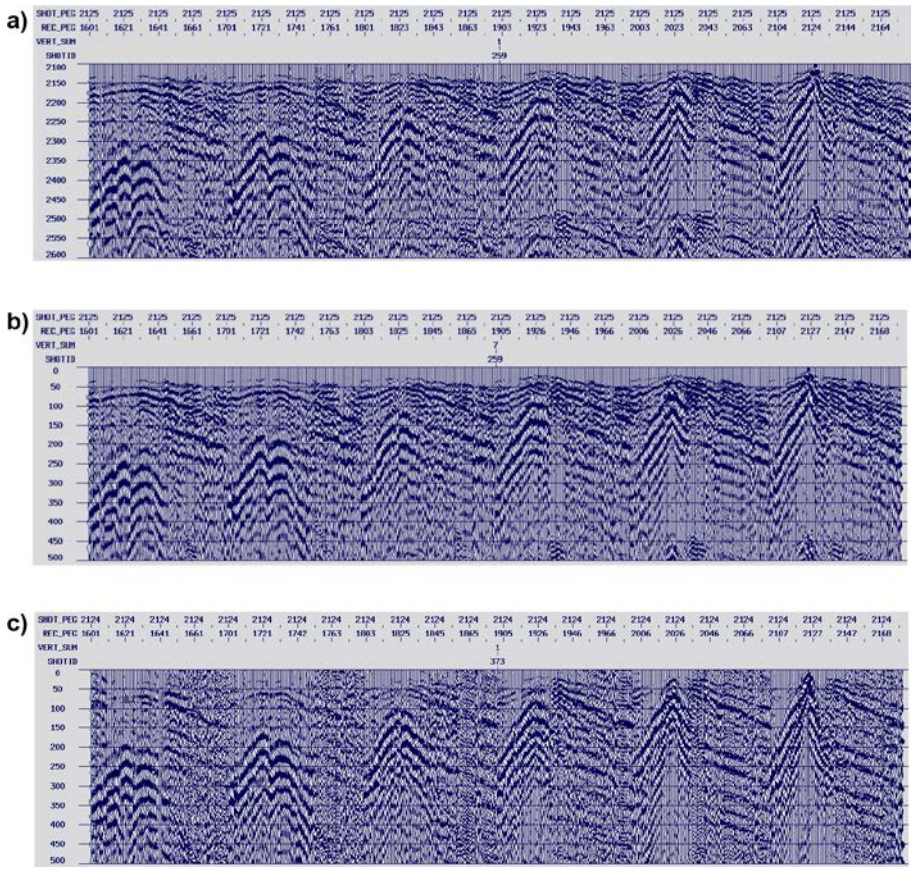

Figure 2-3. *Raw shot-gathers (AGC 500ms applied) from a) 1 Bobcat hit b) 7 stacked Bobcat hits and c) explosive shot.*

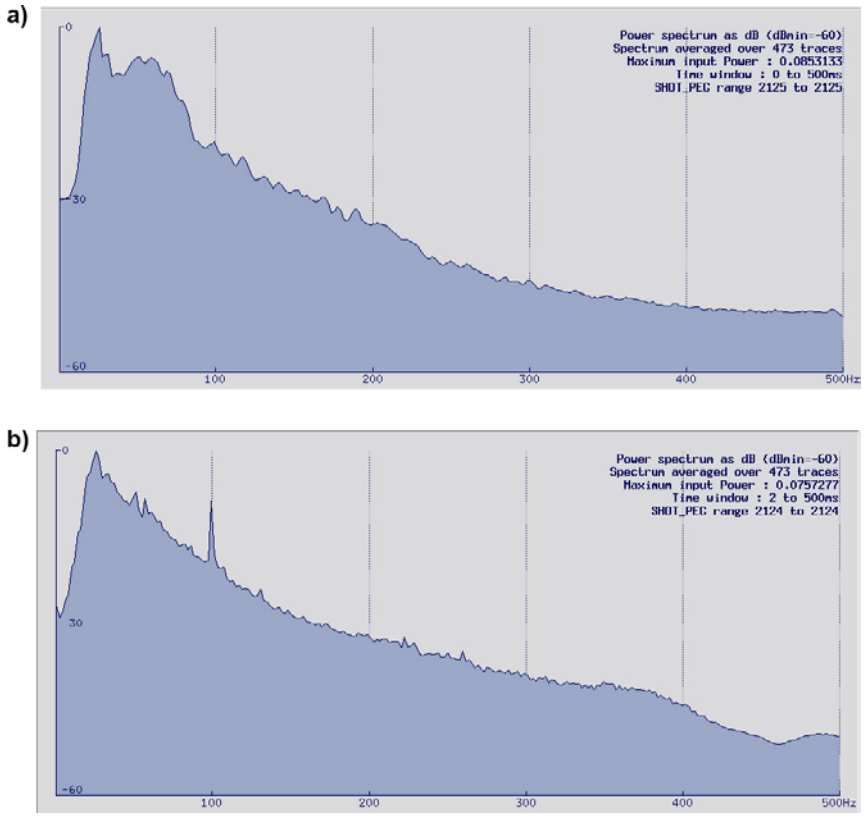

Figure 2-4. *Frequency spectrum graph from a) 7 stacked Bobcat hits and b) explosive shot (Figure 3-3).*

Table 2-1. Seismic acquisition parameters.

Survey parameters	
Acquisition type	3D survey – 4 patches of 6 receiver lines, 80 receivers on each line. No overlap of receiver lines.
Shotlines	Along receiver line in each patch plus three lines on each side of the patch, creating an overlap between patches.
Receiver interval	4 m inline direction/ 14 m crossline direction.
Shot interval	16 m inline direction/ 14 m crossline direction.
Maximum source-receiver offset	~340 m, some shots with larger offsets outside of normal patch shot pattern were done.
Source (open area)	Bobcat mounted weight drop ~500 kg. 10 hits stacked on each shot point.
Source (forest)	Explosive, dynamite charge size 40–80g.
Sensor	~ 400 1C 10 Hz cabled + ~100 1C 10 Hz wireless.
Recording parameters	
Acquisition system	Sercel 428 (GPS time stamping/sampling).
Record length	30 s to ensure 10 Bobcat hits per record.
Sampling rate	1 ms.
Position surveying	
Method (open area)	DGPS (every receiver and shot point, occasionally interpolated in between).
Method (forest)	Total station (every receiver and shot point, occasionally interpolated in between).

3 Data processing

First step in the seismic data processing is picking of first breaks. The first breaks are the travel times of the direct or refracted seismic wave, between the shot point and the receivers. These travel times are used in the refraction and the tomography processing. All travel times have been picked using a semi-automatic approach and picks are then corrected manually, all first breaks are plotted in Figure 3-1. Bobcat shots and explosive shots show similar travel times. Most picks plot along a trend line of 5 300 m/s indicating refracted arrivals from bedrock. The near offsets show a slightly larger spread indicating variations in the depth to bedrock as well as in the velocities in the sediments.

Tomography, refraction processing and reflection processing are complementary methods used to process seismic data. Refraction processing uses the travel times of direct and refracted seismic waves to estimate depth to layer boundaries and velocity changes within the layers. Refraction processing was applied along the receiver lines and hence in 2D. The reason for this is the much denser receiver spacing in inline direction. The 14 m spacing in crossline direction is too coarse to resolve any near surface velocities, which are essential to estimate the depth to bedrock. The 2D refraction processing can, therefore give a better accuracy than 3D refraction processing, in those parts that are well covered by several shot points. However, 3D effects are neglected, which may need to be accounted for when interpreting the data. Furthermore, those parts that are not covered by shot points will be poorly resolved. In the data processing, both two and three layered models were used, with the deepest layer being the bedrock, and upper or upper two layers being sediments. Both kinds of models gave very similar results concerning the depth to bedrock indicating that it is well resolved in the data. The refraction processing uses a generalized linear inversion algorithm based on the reciprocal time differences, slopes and intercepts of travel time-distance plots (see for example Hampson and Russel 1984, Palmer 2010). Starting models were set with the first layer(s) having a velocity in the range of 600–2 500 m/s and the bedrock layer having a velocity in the range of 4 500–6 000 m/s. These boundaries could later during the iterative inversion process be loosened to optimize the data fit. Output from the 2D refraction is a set of node locations (coordinate and depth) for the sediment/bedrock interface. These can then be compared with depth points from geotechnical drilling. Refraction processing also provides a set of nodes for bedrock velocity.

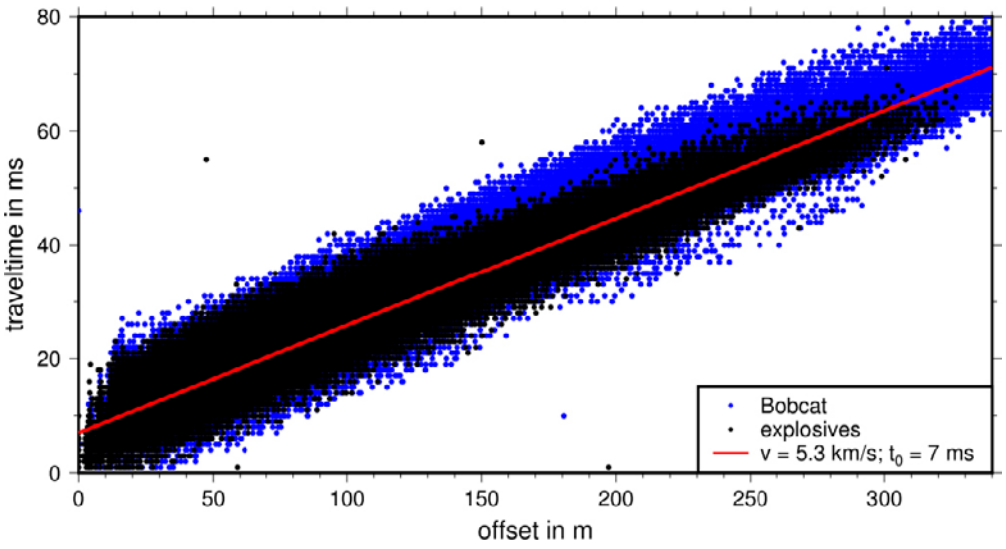

Figure 3-1. *All First arrival picks. Most picks plot around a trend line of 5 300 m/s.*

In tomography the subsurface is divided into cells and each cell is given a starting velocity. Ray tracing is performed where each ray will pass through a finite number of cells. A travel time can then be calculated for each ray and the travel time through the model for each ray is compared with the real travel time of the ray (our data). The velocity in the cells is then updated and a new raytracing performed. The model is updated until the misfit between data and model is minimized. The cell size can be defined depending on the parameters used in the acquisition of the data. A cell size of 2 m in the vertical direction and 4×4 m in horizontal directions were used on the Forsmark 3D data set. The tomography model is smoothed in order to speed up the inversion and to avoid blocky models, but it is also a fundamental part of the forward solver and can, therefore, not be omitted. Details about tomography inversion program and its use can be found in Tryggvason and Bergman (2006) and Tryggvason et al. (2009). Due to the smoothed tomography models, defining the bedrock boundary is not straightforward. Checking the velocity in the tomography model from known bedrock depth points such as those from drilled boreholes is a way to estimate the velocity in the model that corresponds to bedrock depth. By this method one can estimate the depth to bedrock where there are no drilled boreholes. This approach has been used in for example Malehmir et al. (2015) and in the previous seismic study in Forsmark 2011 (Brojerdi et al. 2014).

The model and data fit is measured by the model RMS in both of these processing schemes. However, it is also important to check the location of receivers and shot points before judging the accuracy of the data. Sometimes if there is only few shot points and hence little data the misfit can also be low, however, this does not mean the models are more accurate in that area. Since the RMS values have been low in all our models, the accuracy of the models have been judged based on the density of receivers and shot points as well as on the distribution of shot azimuth.

The last method of processing (reflection processing) uses the seismic energy that is reflected off of boundaries in the subsurface. In Forsmark bedrock is located at a very shallow level most often less than 5 m below surface. With the receiver spacing used in the acquisition in Forsmark 3D, it is not possible to image the reflections from the bedrock. The aim of the reflection processing is to image deeper reflections from deformation zones and lithological boundaries within the bedrock. The reflection processing can give complementary information on the dip of deformation zones (low velocity zones) or structures in the bedrock (e.g. Juhlin 1995).

Reflection processing steps have approximately followed the steps used for previous seismic lines acquired in Forsmark (Juhlin et al. 2002, Juhlin and Palm 2005, Brojerdi et al. 2014). The CDP bin size is 2 m in inline direction and 7 m in crossline direction (Figure 2-2). Due to the large difference in inline/crossline CDP spacing processes, such as Dip Moveout and Migration, can produce artefacts in the data. A cautious processing approach has been used in order to minimize the risk of enhancing artefacts in the data. Also post stack coherency filtering was avoided in order to not emphasize potential artefacts. Fold varies between 30 and up to about 130 in most of the CDP's (Figure 3-2). Much of the reflectivity seen in the stacked 3D seismic data occurs in upper 80 ms. Therefore, there is a risk of stacking energy from refracted P- or S-waves. Effort has, therefore, been put into correlating reflections in stacked section with reflections in shot-gathers. However, reflections have not been easy to see in shot-gathers. Some reflections can only be seen in CDP super-gathers, where traces from several neighbouring CDP's are collected. Processing steps are shown in Table 3-1.

Table 3-1. Reflection seismic data processing flow.

Step	Task
1	Read SEGD data.
2	Trace edit.
3	Add geometry 2 m × 7 m bins.
4	Pick first breaks.
5	Spectral equalization 100-120-240-300 Hz. Window 30 Hz.
6	AGC 50 ms.
7	Refraction static corrections.
8	Datum static corrections.
9	LMO static corrections.
10	Mute first breaks.
11	Mute Shear waves.
12	Mute offsets 0–30 m.
13	Normal Moveout after velocity analysis.
14	Stack.

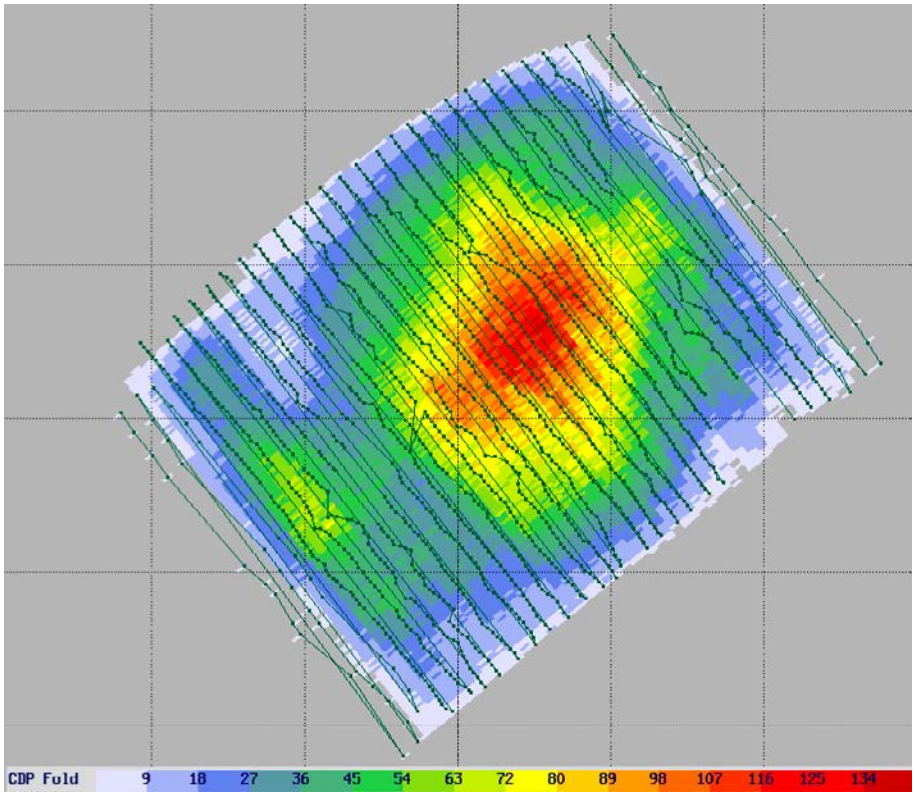

Figure 3-2. *Fold distribution overlaid by receiver positions.*

4 Results

The complete results were sent to SKB separately. The results constitute the interpreted bedrock depth, sometimes referred to as bedrock elevation (expressed in m above sea-level, m.a.s.l.) as well as bedrock velocities at bedrock depth. Also the final reflection 3D stacked seismic data is part of the result. Bedrock depth can be used directly. Bedrock velocities need to be integrated with bedrock geology and other geophysical data before a complete interpretation can be made. Also for reflections, integration with geology and especially deep boreholes is necessary for a complete interpretation. Refraction processing results are delivered in the format x, y, z (Easting coordinate, Northing coordinate, Height) for the top of the bedrock. Refraction processing also produces information of bedrock velocity. Velocity information are in form of nodes and is, therefore, delivered in similar format x, y, v (Easting coordinate, Northing coordinate, Velocity). The velocity nodes are sparser than nodes for the depth and are not located at the same x, y coordinates. Tomography results are in the form of $4 \times 4 \times 2$ m cells. Velocities for all cells are delivered in the format x, y, z, v (Easting coordinate, Northing coordinate, Height, Velocity), where x, y coordinates are from the centre of each cell and height corresponds to top of the cell. Depth to bedrock is also plotted on top of tomography result from the 2D refraction lines with existing boreholes on top. These figures are provided along with the data delivery. Reflection data is delivered in SEGY format, both the raw data and the processed data.

Based on the 2D refraction lines the bedrock depth varies between approximately 3 m above sea level down to about 7 m below sea level (Figure 4-1). Areas where very few first arrivals have been incorporated in the modelling or if only shots in one direction were available, have been plotted in paler colours since the models are less reliable there. Deeper bedrock elevations between 4 and 8 m below sea level occur mainly in the northern corner of the 3D area. This is in good agreement with the bedrock depth from geotechnical boreholes, although the boreholes are sometimes slightly shallower. When regolith depth is less than 2 to 4 m, it is difficult to resolve the bedrock topography with the receiver spacing used in the 3D survey. Geotechnical boreholes are plotted as circles on top of the refraction depth map in Figure 4-1. Overall bedrock depth from boreholes and from 2D refraction processing shows similarities, showing a narrow zone from north to south with lower bedrock elevations. In Figure 4-2 the static corrections from reflection processing is shown on a map. These corrections are calculated in 3D using the same travel times as used in tomography and 2D refraction. Large static corrections indicate a thicker sediment layer. The refraction static corrections map shows similar trend as 2D refraction (compare Figures 4-1 and 4-2). These two maps can be compared since the elevation difference in the area is small.

Due to smoothing during tomography processing, the bedrock depth in the tomography model cannot be picked from the bedrock velocity (around 5 300 m/s). Instead extracting the velocity from a known depth point, such as those given by geotechnical boreholes, will give an idea of the model velocity at the bedrock depth. Velocities were extracted from a radius of 3 m around each borehole in the 3D seismic area. Boreholes where the regolith depth was less than 4 m were neglected. Velocities are in the range of 1 500 to 3 500 m/s with a slight increase in velocity at larger bedrock depths. Average velocity is 2 700 m/s. This is in agreement with previous tomographic results in Forsmark (Brojerdi et al. 2014), where a velocity of about 3 000 m/s from tomography model gave good correlation with boreholes depth and refraction processing.

Figure 4-3 shows the velocities from tomography model extracted at borehole depth. Low bedrock velocity may indicate fractured bedrock. Figure 4-4 shows the bedrock velocity from the refraction processing. The lowest bedrock velocities occur in the northern corner of the 3D area and also towards the south. In most areas bedrock velocity is lower where bedrock elevation is also at a deeper level or sediment is thicker, compare Figures 4-1 to 4-4. Low bedrock elevation and low bedrock velocity is most prominent in the northern corner and continuous in a narrow zone towards south. The bedrock in the area is mostly granitic (average velocity around 5 300 m/s, Figure 3-1). Velocity estimation from the 2D refraction processing may not give exact velocities and especially narrow low velocity zones may appear as a wider zone with a slightly lowered velocity. Therefore, checking the velocity variations also from the tomography is helpful for determining where low velocity zones occur. Figure 4-5 shows results from line 23. In the northern part of line 23 velocities from the tomography model are significantly lower than average below the expected bedrock depth (results from refraction processing, dashed line), indicating higher fracture intensity.

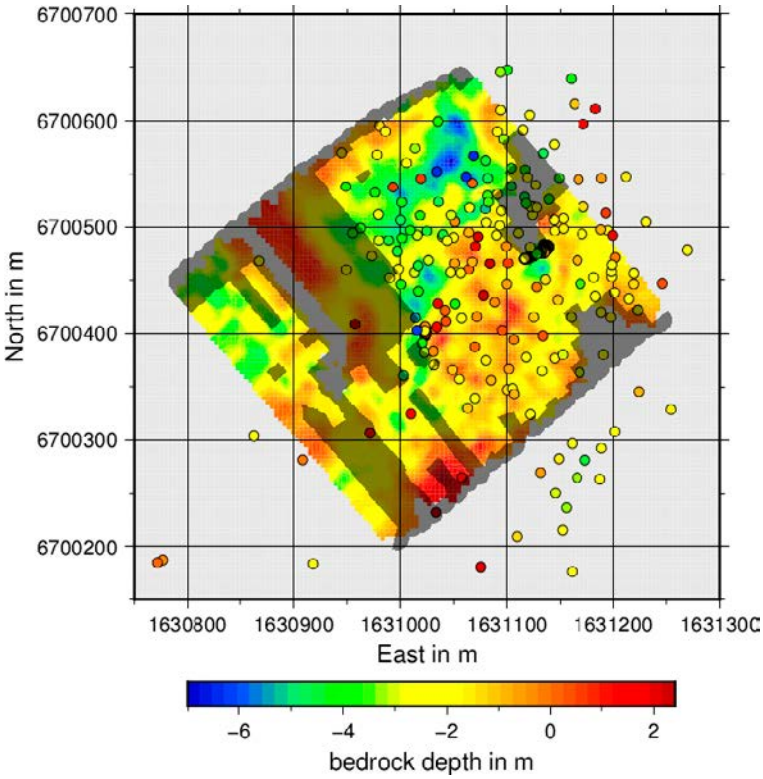

Figure 4-1. *Bedrock depth, in m.a.s.l from refraction processing. Uncertain areas have been plotted in paler colour. Circles show bedrock depth from geotechnical boreholes.*

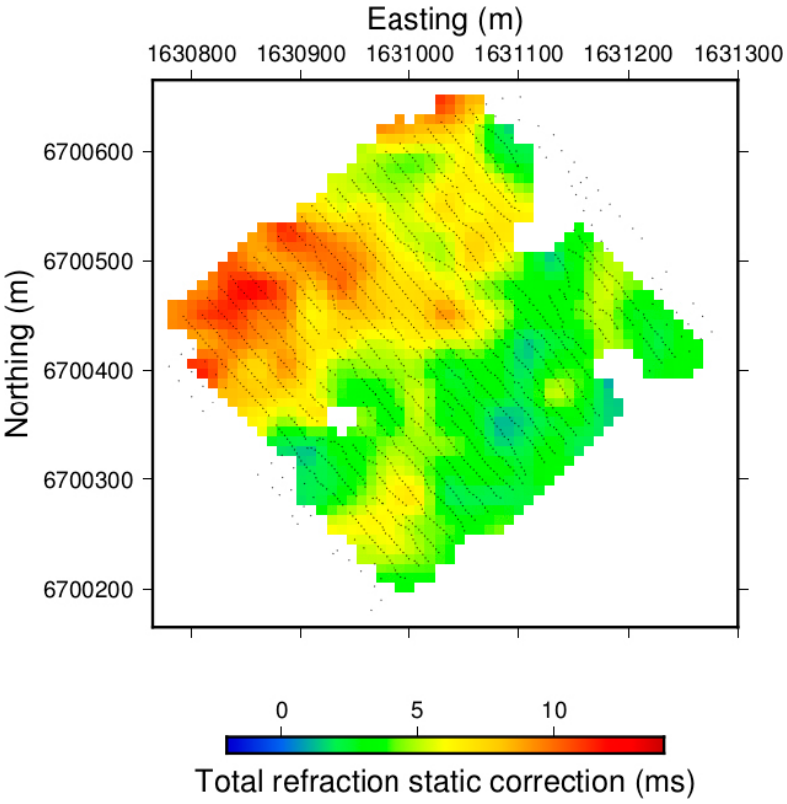

Figure 4-2. *Static corrections from 3D refraction static calculations. Larger static correction indicates a thicker sediment layer.*

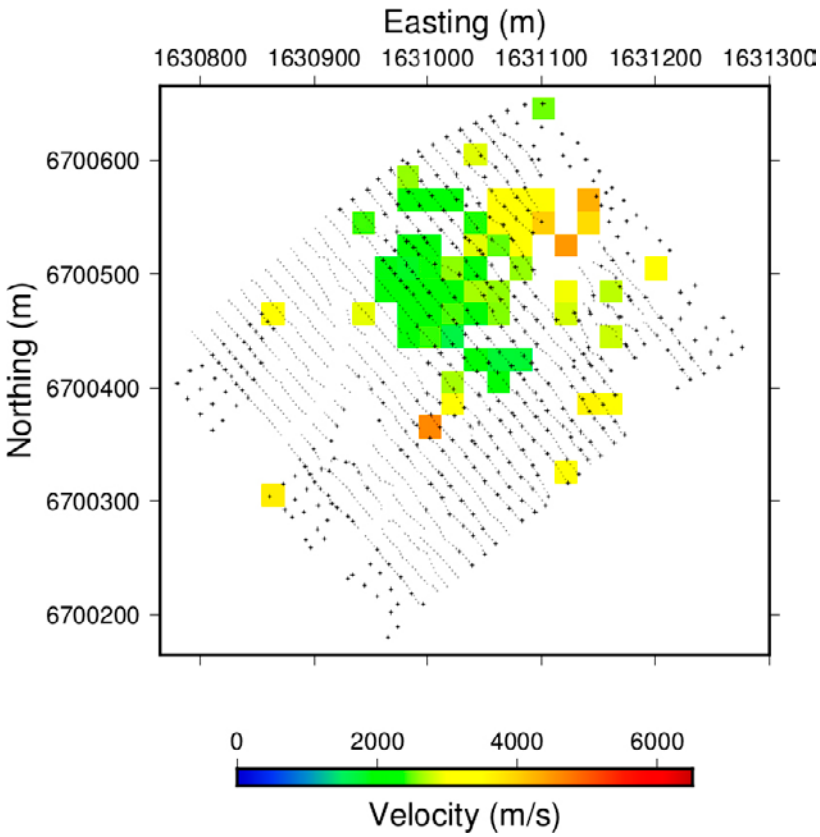

Figure 4-3. *Bedrock velocity from tomography model extracted at borehole depth.*

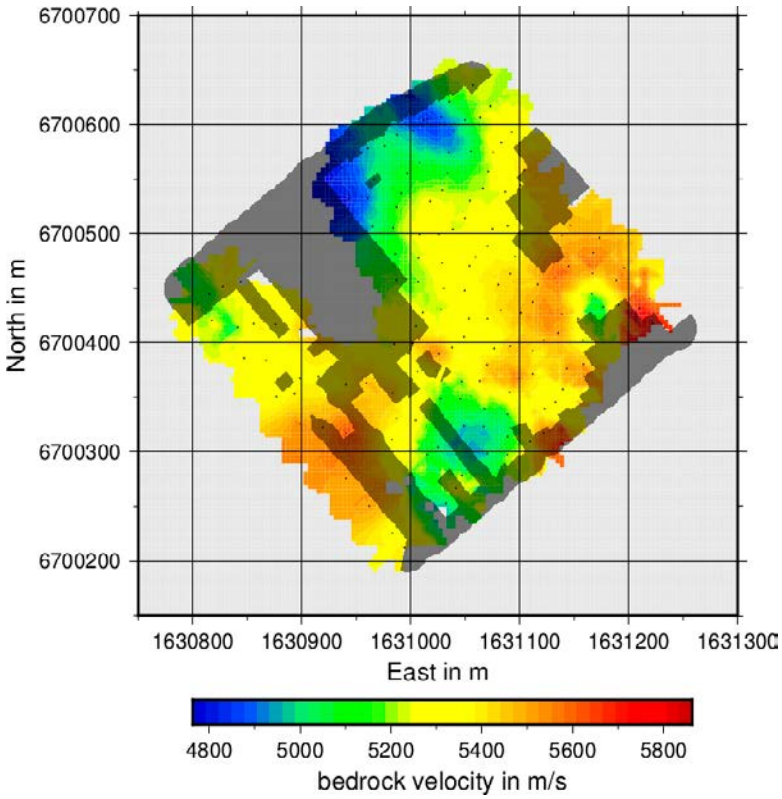

Figure 4-4. *Bedrock velocity from refraction processing. Uncertain areas have been plotted in paler colour. Black dots mark the node locations.*

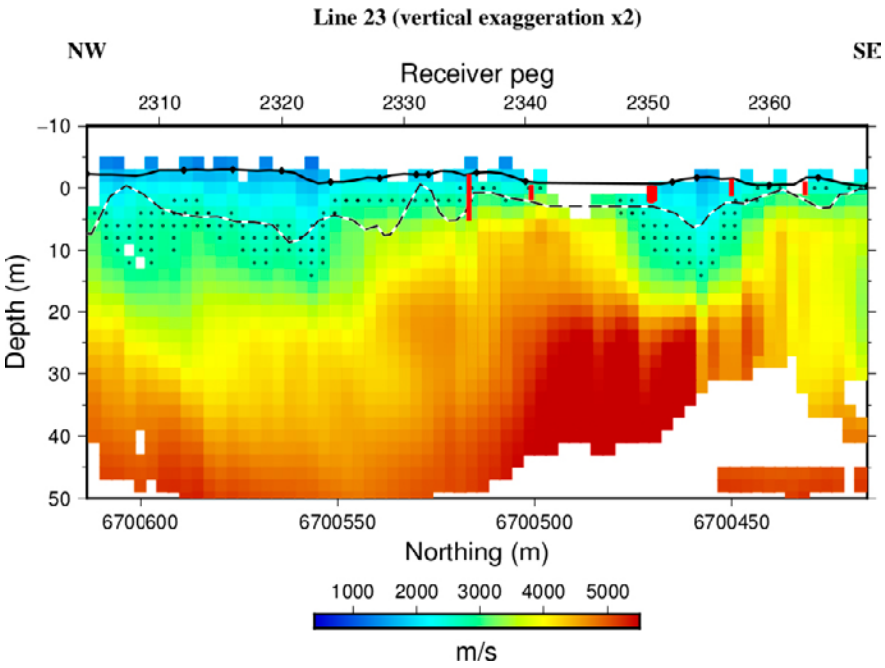

Figure 4-5. *Refraction and tomography results from line 23. Dashed black and white line show bedrock depth from 2D refraction model. Coloured cells show the velocity from the 3D tomography model, cells with a velocity in the range 2 500 to 2 900 m/s are marked with a small circle. Red lines show bedrock depth from boreholes.*

In general, reflections were difficult to distinguish directly from shot-gathers. Figure 4-6 a) shows a raw shot-gather, b) shows the same shot-gather after applying static corrections and c) shows the same shot-gather after spectral equalization. In this shot-gather reflection R4 can be identified. Figure 4-6 d) shows the same shot-gather after muting of direct and refracted waves as well as surface waves. Reflection R4 is still visible. Other reflections could be identified in CDP super gathers (Figure 4-6). In Figure 4-7, reflections R1 to R3 can be identified. The reflections are visible after static corrections and spectral equalization have been applied and are still visible after muting of direct and refracted waves as well as surface waves. Reflections R2 to R4 appear as distinct reflections whereas reflection R1 appears as a set of reflectivity. The approximate depth of reflections R1 to R4 can be estimated based on the travel times and using a bedrock velocity of 5 000 m/s for converting travel times to depth. The approximate depth to corresponding reflectors for the identified reflections is shown in Table 4-1. In Figure 4-8 areas where these reflections are observed in shot- or CDP gathers are marked. Such observations are certain, but the reflections can be traced over a larger area in the stacked sections.

Table 4-1. Identified reflections.

Reflection	Zero offset time (ms)	Approximate depth (m)
R1	45–80	100–200
R2	30–35	75–90
R3	~ 40	~ 100
R4	~ 25	~ 60

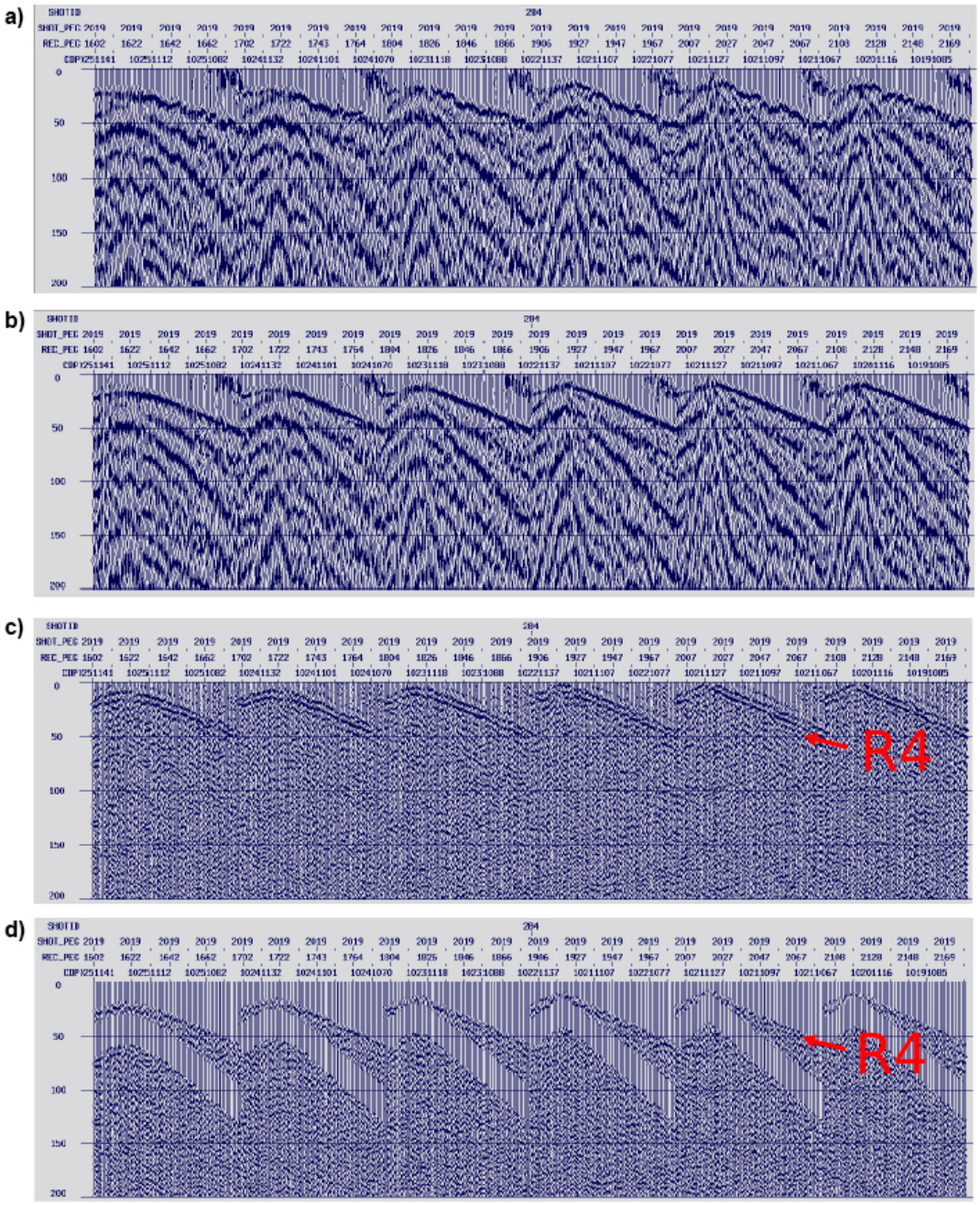

Figure 4-6. *Shot-gather from line 20 a) raw b) after static corrections c) after spectral equalization and d) after muting first arrivals and shear waves. AGC 50 ms applied in all shot-gathers. Reflection R4 is visible in processed shot-gather.*

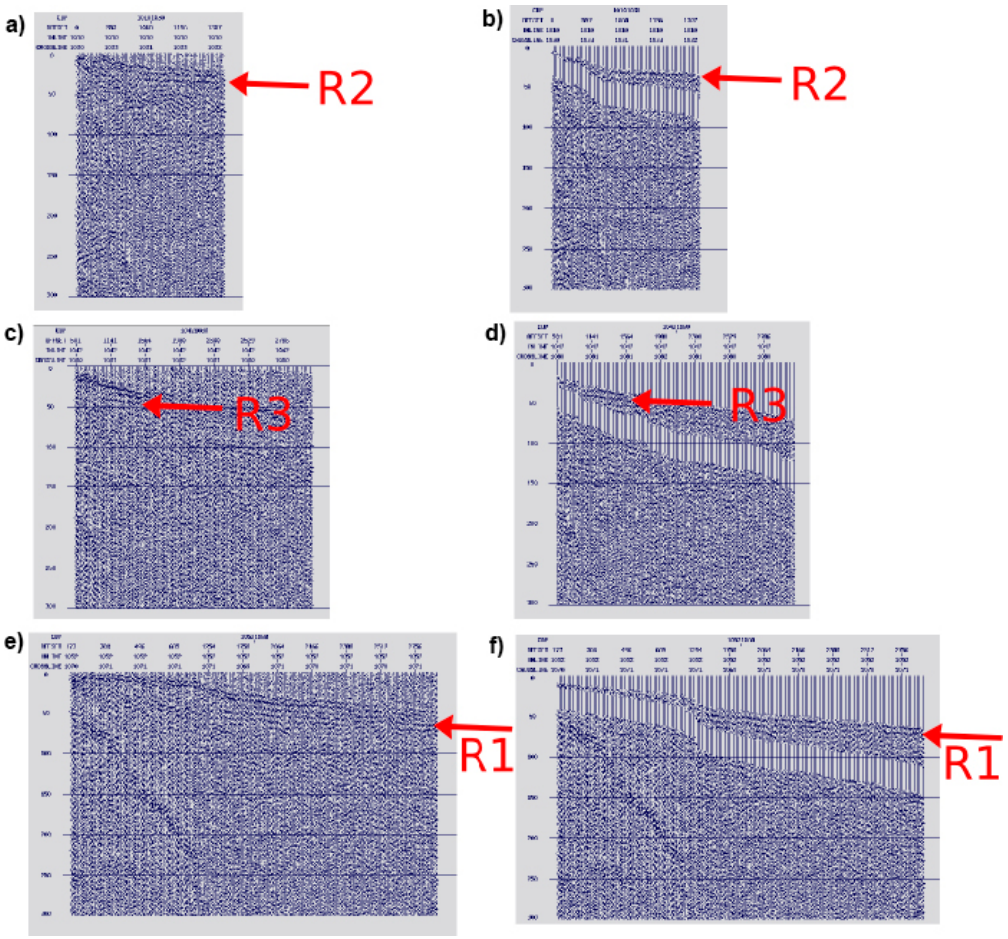

Figure 4-7. *CDP super gathers from a) CDP 10101030, reflection R2 visible b) same as a) after removal of first arrivals and shear waves, c) CDP 10421080, reflection R3 visible, d) same as c) after removal of first arrivals and shear waves, e) CDP 10501070, reflective package R1 visible, f) same as e) after removal of first arrivals and shear waves.*

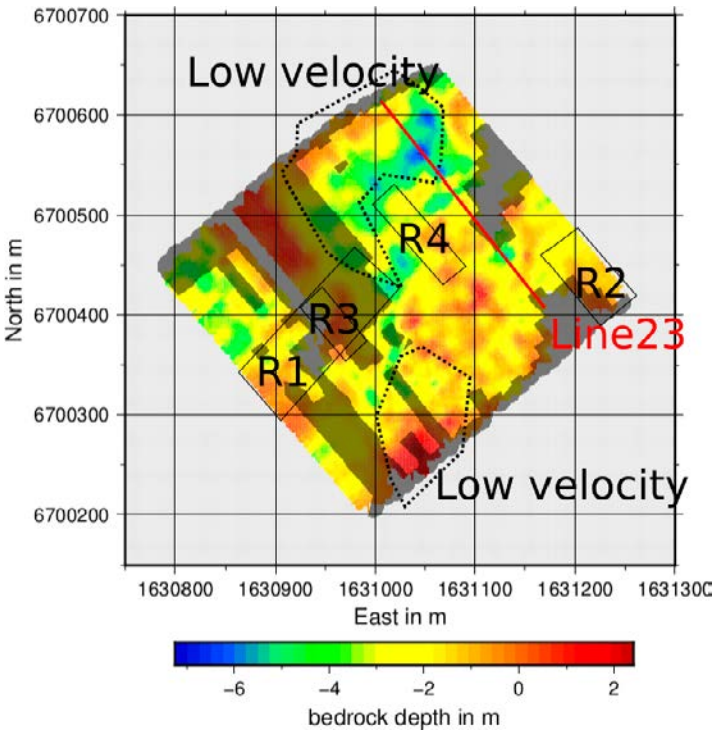

Figure 4-8. *Summary of results plotted on bedrock depth map. Dotted lines show areas where bedrock velocities are low. These areas partly coincide with deeper bedrock elevations and may indicate fractured bedrock in the near surface. Black squares show where reflections R1 to R4 are identified in shot or CDP gathers. Red line indicates location of Line 23 (Figure 5-5).*

5 Interpretation and discussion

A primary interpretation is presented in this report based on the acquired seismic data and geotechnical drillings (Hansson et al. 2008, Hellgren 2012a, b) and 15 deeper boreholes (Carlsten et al. 2006a; Carlsten et al. 2006b; Carlsten et al. 2007). From the geotechnical boreholes the depth to bedrock has been used for comparison with refraction and tomography results. From the deep boreholes interpreted intersections between fracture domains (FFM01 and FFM02) have been compared with reflections in the 3D stacked data. Figure 4-5 shows tomography model (coloured cells) and refraction bedrock depth (dashed black and white line) from line 23. This line is well covered by seismic data and also has several boreholes to compare depth with and serves as an example on how this data can be interpreted. The bedrock depth does not need interpretation, however, it is important to judge the uncertainties in the data. In Figure 4-1 uncertain areas are plotted with a paler colour scale. These are areas with poor shot/receiver coverage and/or shots in only one direction. In general the bedrock depth from refraction processing sometimes shows slightly deeper bedrock level than from boreholes. Possible explanations for this are:

- Unresolved low velocity layer near surface may push down the bedrock in the refraction modelling.
- Severely fractured bedrock near surface may be interpreted as sediments in refraction processing.
- Drilling into large boulders may be interpreted as bedrock during drilling although real bedrock is at a deeper level.
- If rapid variations in bedrock depth occur, misplaced coordinates from drilling or from seismic acquisition may cause different bedrock level.

Some gaps occur along line 23 and here the depth to bedrock is less constrained. In areas with little or no data, the refraction depth is usually linearly interpolated or no depth nodes are calculated. Tomography may show empty cells in the near surface since no rays have penetrated this area. In general the depth from refraction processing correlates well with borehole depth along line 23. Next step is to evaluate if there are any low velocity zones in the bedrock. Low velocity zones may indicate fractured rock. Two zones occur in line 23 where bedrock velocity from tomography below the bedrock depth is significantly lower than average. The zone in the south-eastern part of the line reaches high velocity (5 000 m/s) in the tomography model at about 20 m below sea level. This velocity indicates solid rock. However, in the north-eastern part of the line, low velocity penetrates much deeper and even at 50 m below sea level velocity is not above 4 500 m/s. This may indicate that the upper 30 - 40 m of the bedrock is fractured. Based on inspection of tomography models an area with low bedrock velocities has been outlined in Figure 4-8. The low velocity zone partly correlates with lower bedrock elevation. Fractured rock in the upper part of the bedrock is most likely in the northern corner, but may continue in a narrow zone towards south.

In the deeper part, interpretations are made based on reflection processing. Previous seismic data (Brojerdi et al. 2014) found a possible correlation between a reflection at about 60 m depth (G8 reflection) and the shallow dipping deformation zone ZFM1203. In the 3D seismic data one reflection, R4, has been found at approximately 60 m depth. This reflection is seen in shot gathers around the inlines 1020 to 1025 between crosslines 1060 to 1100. The reflection can possibly be extended further in the stacked sections and a shallow reflection at about 60 to 80 m depth is visible in most inlines. It is, however difficult to trace it across the 3D area. Assuming the R4 reflection originates from the ZFM1203 structure, a dip of about 8° gives a good fit with the R4 reflection. Notice that this modelling is different from the modelling that was used in the 2011 seismic investigation, in terms of dip and orientation of structure. It was also suggested that the reflectivity could originate at an interface between fractured rock and intact rock. In Figures 5-1 to 5-8, sections of 3D stacked seismic data is shown. Yellow squares mark points of intersections, interpreted from deep boreholes, between fracture domain FFM01 and FFM02. The red line marks the modelled location of ZFM1203. Surface location from where ZFM1203 was modelled is shown in Figure 5-9. It seems to be a good correlation between uppermost reflectivity in the stacks and the fracture domain intersections in many cases (Figures 5-1, 5-2 and 5-6). In other cases, however, R4 correlates better with the modelled ZFM1203 (Figure 5-5). It seems that the fracture domain intersections correlate well with

the uppermost reflectivity in the stacked section and most stacked sections show reflections also at a deeper level for example reflections R1 to R3 that clearly are not related to the fracture domain intersections. Possible explanations for the deeper reflections are:

- Other fracture domain boundaries at deeper level.
- Lithological contacts.
- A Deformation zone (possibly extension from ZFM1203).

Difficulty to trace reflections in other areas may be due to noise in some areas or due to low fold, (see Fold distribution in Figure 3-1). Possibly low velocity zones if consisting of fractured rock may disturb the reflected energy in these areas.

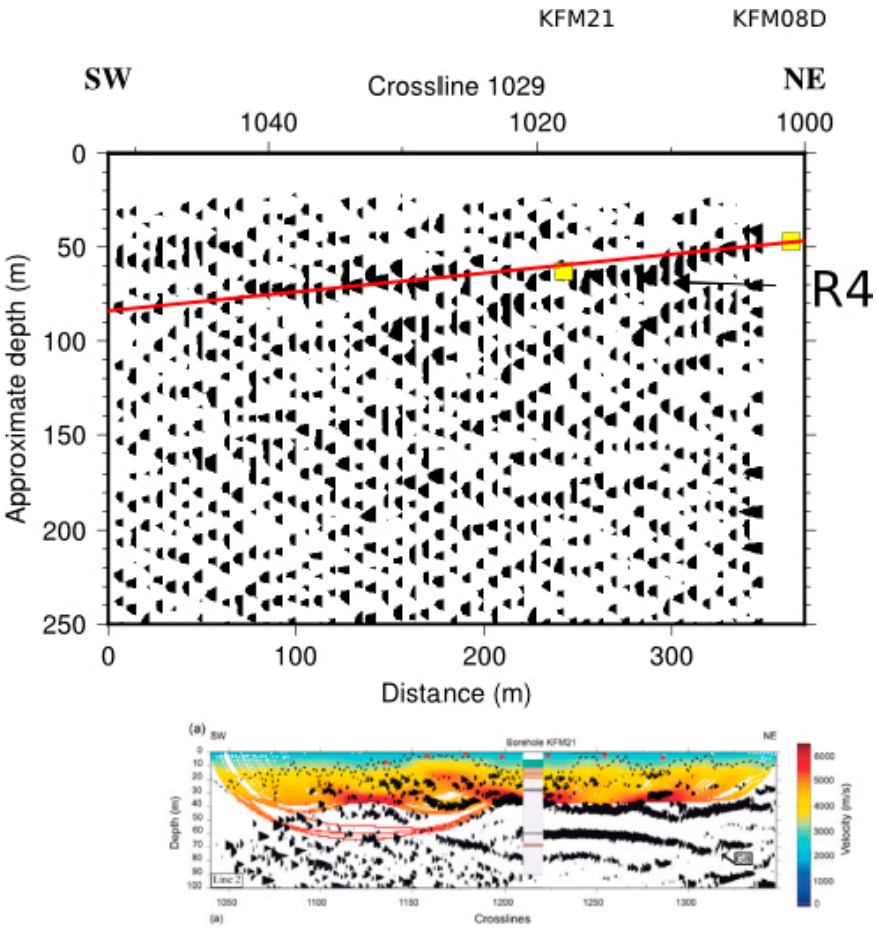

Figure 5-1. *A comparison between 3D seismic (crossline 1029, upper) and previous seismic Line 2 from 2011 (Brojerdi et al. 2014). The 3D seismic crossline spacing is 7 m compared with 1 m in the previous data. Post stack coherency filtering has been applied to 3D data for enhancing reflections. Modelled 8° northwest dipping structure marked in red. Yellow squares mark points of intersections between fracture domain FFM01 and FFM02.*

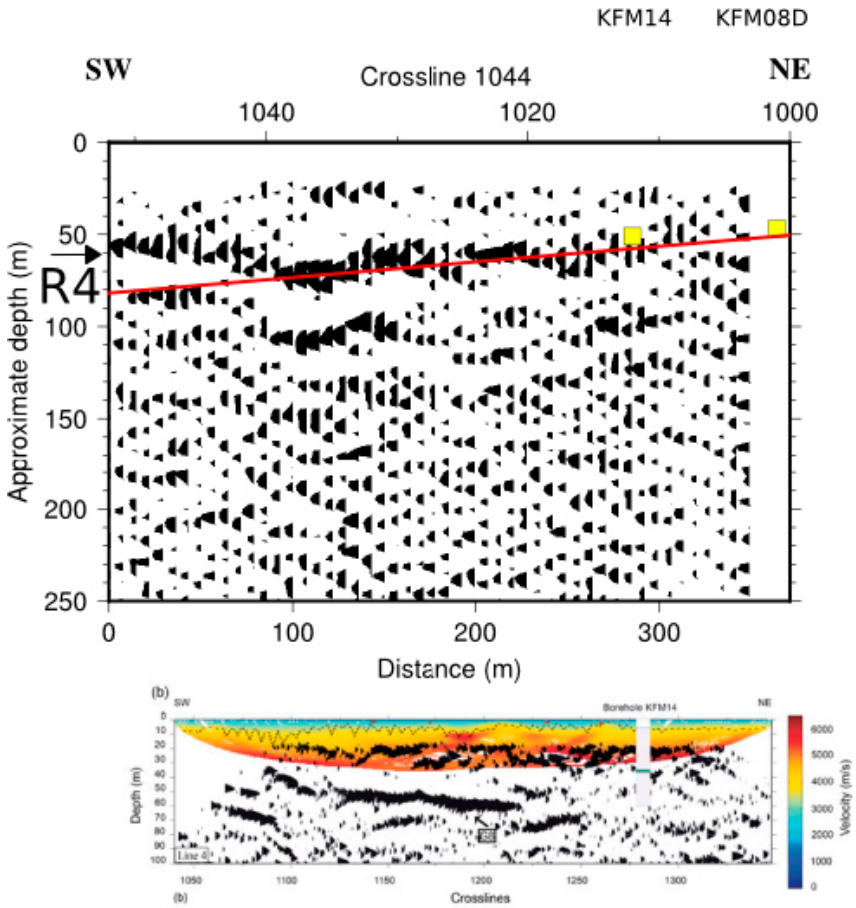

Figure 5-2. *A comparison between 3D seismic (crossline 1044, upper) and previous seismic Line 4 from 2011 (Brojerdi et al. 2014). The 3D seismic crossline spacing is 7 m compared with 1 m in the previous data. Post stack coherency filtering has been applied to 3D data for enhancing reflections. Modelled 8° northwest dipping structure marked in red. Yellow squares mark points of intersections between fracture domain FFM01 and FFM02.*

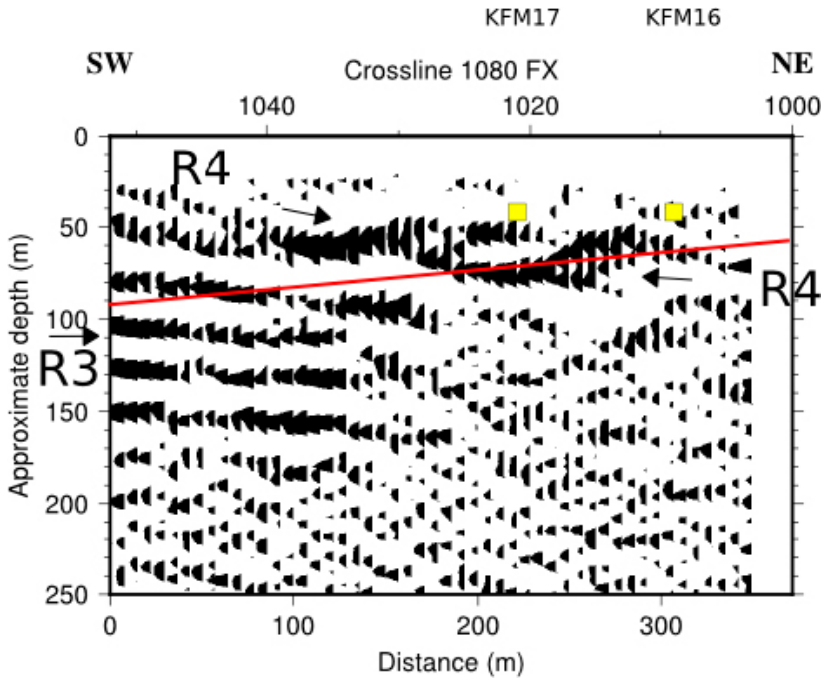

Figure 5-3. *Crossline 1080. Reflections R3 and R4 marked with arrow. Modelled 8° northwest dipping structure marked in red. Yellow squares mark points of intersections between fracture domain FFM01 and FFM02.*

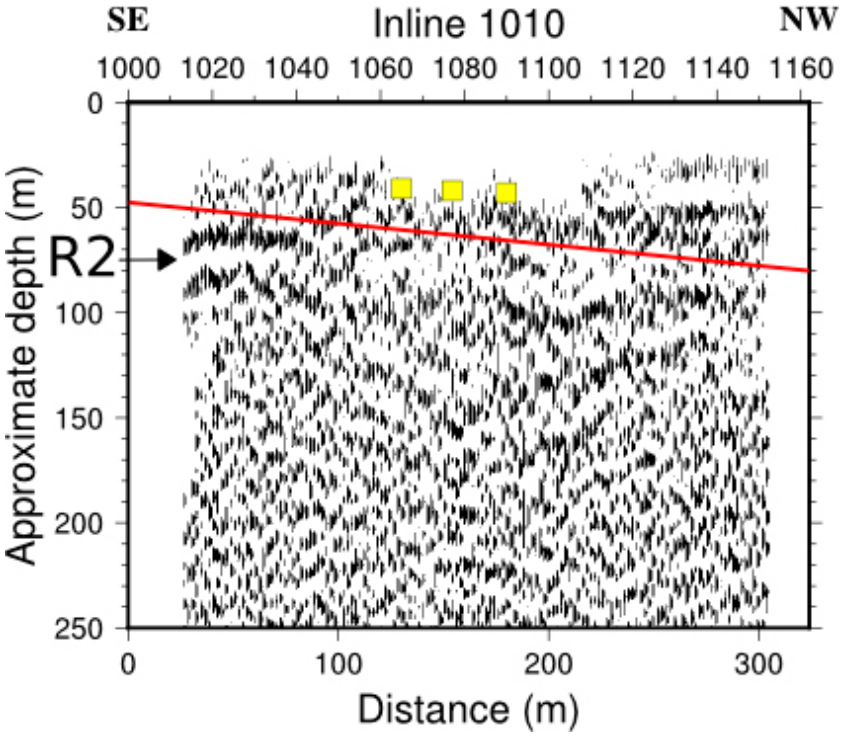

Figure 5-4. *Inline 1010. Reflection R2 marked with arrow. Modelled 8° northwest dipping structure marked in red. Yellow squares mark points of intersections between fracture domain FFM01 and FFM02.*

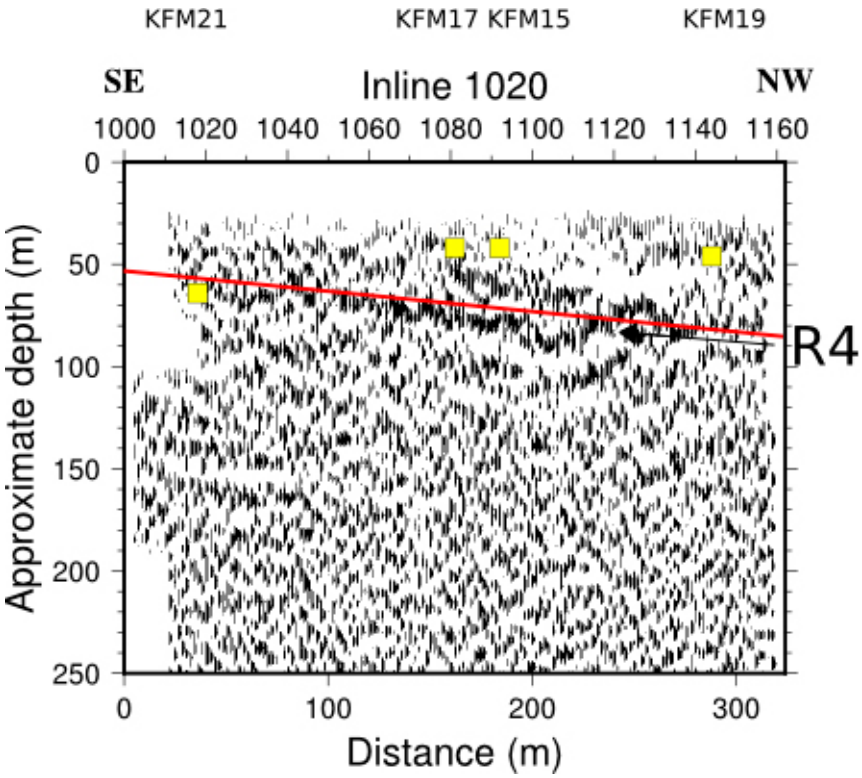

Figure 5-5. *Inline 1020. Reflection R4 marked with arrow. Modelled 8° northwest dipping structure marked in red. Yellow squares mark points of intersections between fracture domain FFM01 and FFM02.*

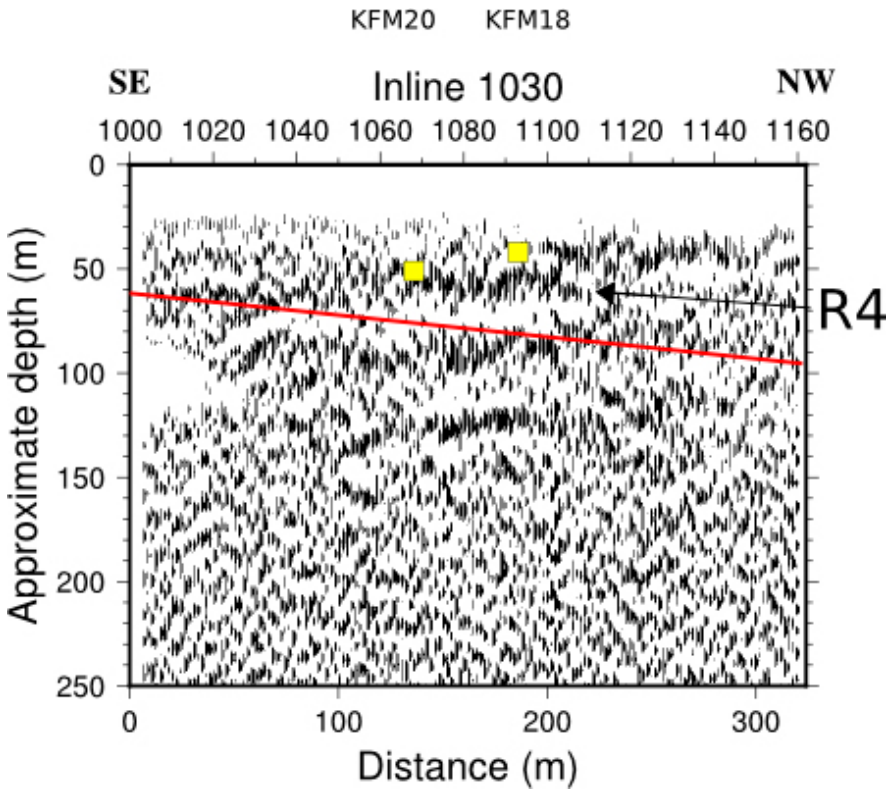

Figure 5-6. *Inline 1030. Reflection R3 marked with arrow. Modelled 8° northwest dipping structure marked in red. Yellow squares mark points of intersections between fracture domain FFM01 and FFM02.*

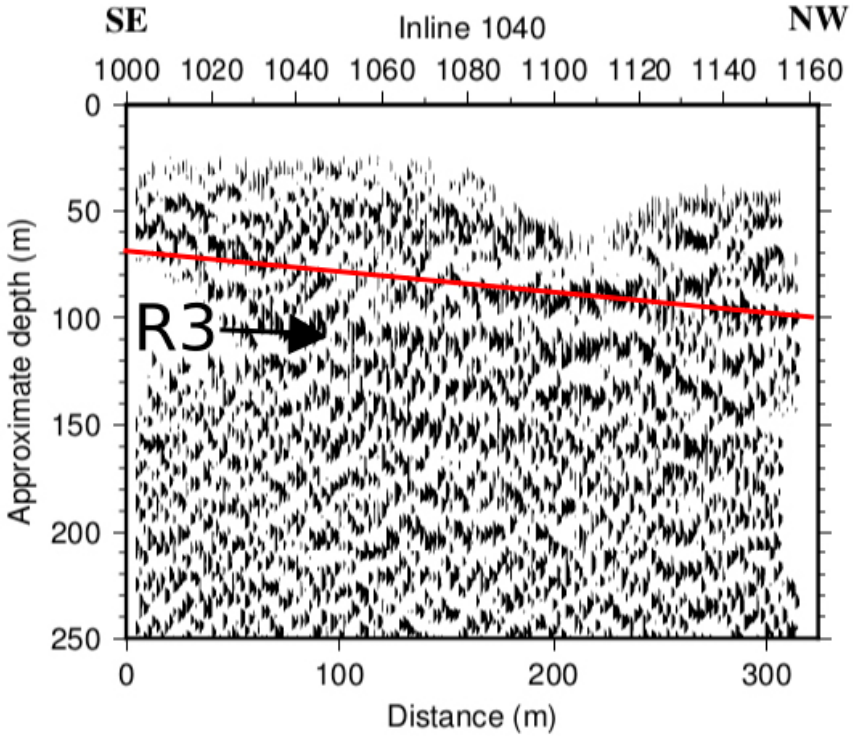

Figure 5-7. *Inline 1040. Reflection R3 marked. Modelled 8° northwest dipping structure marked in red.*

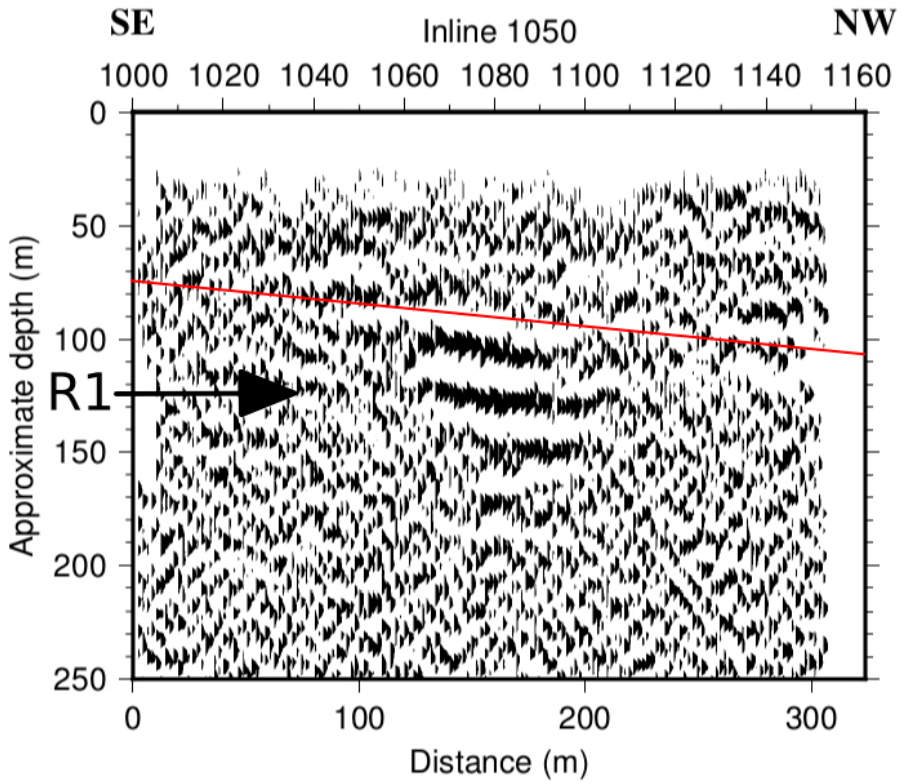

Figure 5-8. *Inline 1050. Reflection R1 marked. Modelled 8° northwest dipping structure marked in red.*

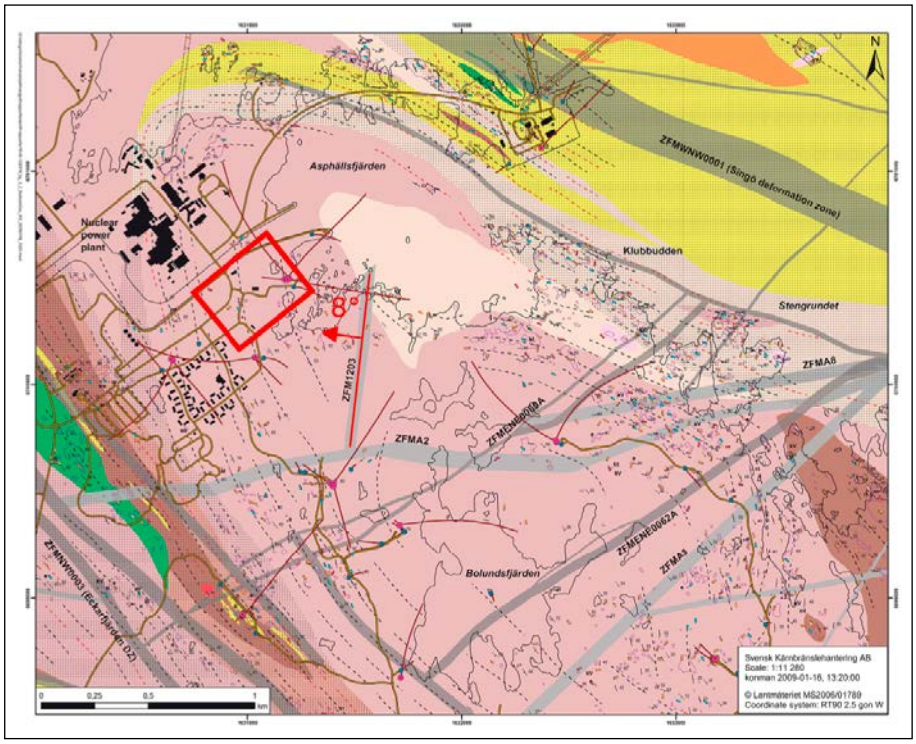

Figure 5-9. *Geological map showing ZFM1203 and its relation to 3D seismic location. A structure dipping 8° towards northwest can fit some of the reflectivity in the 3D seismic data. Coordinate system: RT90 2.5 gon W.*

6 Conclusions

Bedrock depth varied between 3 m above sea level to 7 m below sea level. Depth were compared with results from geotechnical drilling and showed good agreement in most cases. Deepest sediment/bedrock interface were found in the northern part of the 3D area and in a narrow zone towards south. Low velocity bedrock showed a similar trend with low velocities mainly in the north and in a narrow zone towards the south. Low velocity bedrock may indicate more fractured bedrock. Most reflectivity occurred between 40 and 80 m depth. The uppermost reflectivity is in good agreement with interpreted intersections between fracture domains FFM01 and FFM02. A good correlation also exists between a modelled reflector originating at surface expression of ZFM1203 and dipping 8° towards northwest and reflectivity in the stack. Since the reflections cannot be traced across the 3D area and not be linked directly to ZFM1203 other explanations for the reflectivity must be considered. Other explanations are deeper fracture domains similar to FFM01 and FFM02 or lithological contacts. For a better correlation between reflections and the fracture domain intersections, more intersection points are needed. Also a better knowledge of the velocity structure can improve the stacking of reflections and the depth conversion.

Further mapping of sonic velocities in existing boreholes can help determining the boundary between fracture domains. Logging the seismic velocity also at seismic wavelength by downhole hydrophones can help creating a better depth conversion for the stacked 3D seismic data and, hence get a better image between existing boreholes. This type of velocity information can also give a better starting model for detailed tomography inversions along selected 2D lines with dense shot and receiver spacing.

References

SKB's (Svensk Kärnbränslehantering AB) publications can be found at www.skb.com/publications.

Brojerdi F S, Zhang F, Juhlin C, Malehmir A, Lehtimäki T, Mattsson H, Curtis P, 2014. High resolution seismic imaging at the planned tunnel entrance to the Forsmark repository for spent nuclear fuel, central Sweden. Near Surface Geophysics 12, 709–719.

Carlsten S, Gustafsson J, Mattson H, Petersson J, Stephens M, 2005. Forsmark site investigation. Geological interpretation of KFM08A, KFM08B and HFM22 (DS8). SKB P-05-262, Svensk Kärnbränslehantering AB.

Carlsten S, Döse C, Samuelsson E, Petersson J, Stephens M, Thunehed H, 2006. Forsmark site investigation. Geological single-hole interpretation of KFM08C, KFM10A, HFM23, HFM28, HFM30, HFM31, HFM32 and HFM38. SKB P-06-207, Svensk Kärnbränslehantering AB.

Carlsten S, Samuelsson E, Gustafsson J, Stephens M, Thunehed H, 2007. Forsmark site investigation. Geological single-hole interpretation of KFM08D. SKB P-07-108, Svensk Kärnbränslehantering AB.

Hampson D, Russell B, 1984. First-break interpretation using generalized linear inversion. Journal of the Canadian Society of Exploration Geophysicists 20, 40–54.

Hansson B, Nordén H, Hedman P, 2008. Platsundersökning Forsmark. Kompletterande jord- och bergsonderingar I bostadsområdet. SKB P-08-23, Svensk Kärnbränslehantering AB. (In Swedish.)

Hellgren S, 2012a. RGeo jordbergsonderingar Etapp 1. SKBdoc 1325135 ver 1.0, Svensk Kärnbränslehantering AB.

Hellgren S, 2012b. RGeo jordbergsonderingar Etapp 2. SKBdoc 1325128 ver 1.0, Svensk Kärnbränslehantering AB.

Juhlin C, 1995. Imaging of fracture zones in the Finnsjön area, central Sweden, using the seismic reflection method. Geophysics 60, 66–75.

Juhlin C, Palm H, 2005. Forsmark site investigation. Reflection seismic studies in the Forsmark area, 2004: Stage 2. SKB R-05-42, Svensk Kärnbränslehantering AB.

Juhlin C, Bergman B, Palm H, 2002. Reflection seismic studies in the Forsmark area – stage 1. SKB R-02-43, Svensk Kärnbränslehantering AB.

Malehmir A, Zhang F, Dehghannejad M, Lundberg E, Döse C, Friberg O, Brodic B, Place J, Svensson M, Möller H, 2015. Planning of urban underground infrastructure using a broadband seismic landstreamer – Tomography results and uncertainty quantifications from a case study in southwestern Sweden. Geophysics 80, B177–B192.

Palmer D, 2010. Characterizing the near surface with detailed refraction attributes. In Miller R D, Bradford J H, Holliger K (eds). Advances in near-surface seismology and ground- penetrating radar. Society of Exploration Geophysicists, American Geophysical Union, Environmental and Engineering Geophysical Society. (Geophysical Developments Series 15), 233–249.

Tryggvason A, Bergman B, 2006. A traveltime reciprocity discrepancy in the Podvin & Lecomte *time3d* finite difference algorithm. Geophysical Journal International 165, 432–435.

Tryggvason A, Schmelzbach C, Juhlin C, 2009. Traveltime tomographic inversion with simultaneous static corrections – Well worth the effort. Geophysics 74, WCB25–WCB33.

Arkitektkopia AB, Bromma, 2018

SKB is responsible for managing spent nuclear fuel and radioactive waste produced by the Swedish nuclear power plants such that man and the environment are protected in the near and distant future.

skb.se